https://doi.org/10.5194/gmd-2019-165
Preprint. Discussion started: 22 July 2019

Geoscientific Model Development Discussions

Implementation of a synthetic inflow turbulence generator in idealised WRF v3.6.1 large eddy simulations under neutral atmospheric conditions

Jian Zhong[1], Xiaoming Cai[1*] and Zheng-Tong Xie[2]
[1]School of Geography, Earth & Environmental Sciences, University of Birmingham, Edgbaston, Birmingham, B15 2TT, UK
[2]School of Engineering Sciences, University of Southampton, Southampton, SO17 1BJ, UK

Correspondence to: Xiaoming Cai (x.cai@bham.ac.uk)

Abstract: A synthetic inflow turbulence generator was implemented in the idealised Weather Research and Forecasting large eddy simulation (WRF-LES v3.6.1) model under neutral atmospheric conditions. This method is based on an exponential correlation function, and generates a series of two-dimensional slices of data which are correlated both in space and in time. These data satisfy a spectrum with a near '-5/3' inertial subrange, suggesting its excellent capability for high Reynolds number atmospheric flows. It is more computationally efficient than other synthetic turbulence generation approaches, such as three-dimensional digital filter methods. A WRF-LES model with periodic boundary conditions was configured to provide *a priori* turbulent information for the synthetic turbulence generation method and used as an evaluation for the inflow case. The comparison shows that the inflow case generated similar turbulence structures as these in the periodic case after a short adjustment distance. The inflow case yielded a mean velocity profile in a good agreement with the desired one, and 2nd order moment statistics profiles close to the desired ones after a short distance. For the range of the integral length scale which we tested, its influence on the profiles of the mean velocities is not significant, whereas its influence on the second moment statistics profiles is evident, in particular for very small integral length scales. This implementation can be extended to the WRF-LES simulation of a horizontally inhomogeneous case with non-repeated surface landuse pattern and a multi-scale seamless nesting case from a meso-scale domain with a km-resolution down to LES domains with metre resolutions.

Key words: Inflow turbulence generator, Large eddy simulation, Exponential correlation function, Atmospheric boundary layer.

1 Introduction

Atmospheric boundary layer flow involves a wide range of scales of eddies, from quasi two-dimensional structures at the mesoscale and synoptic scales to three-dimensional turbulence structures (normally with higher Reynolds number, i.e. Re ~10^8-10^9) at the microscale (Munoz-Esparza et al., 2015). The Weather Research and Forecasting (WRF) model (Skamarock and Klemp, 2008) provides the capability of simulating the atmospheric modelling system at a variety of scales. At the

https://doi.org/10.5194/gmd-2019-165
Preprint. Discussion started: 22 July 2019

Geoscientific Model Development Discussions

mesoscale and synoptic scales, the WRF model allows grid nesting for downscaling at different resolutions from 10-100km to 1-10 km using a fully compressible and non-hydrostatic Reynolds-averaged Navier-Stokes (RANS) solver (Nottrott et al., 2014), which captures the behaviour of mean flow only. At the microscale, a large eddy simulation model can be activated in the WRF model (WRF-LES). The WRF-LES model can capture the intermittency of three-dimensional turbulent eddies. There still remains a challenge for downscaling from mesoscale simulation (down to 1 km) to the LES scale (tens of meters or below) (Doubrawa et al., 2018). Consequently, these two scales of problems are studied separately. Most WRF-LES models of atmospheric boundary layer flow at the microscale uses periodic boundary conditions and simplified large-scale geostrophic forcing for idealised simulations. These brave assumptions inevitably bear with a consequence that simulated atmospheric fields using the cyclic conditions and underlying landuse are interpreted to have repeated features and this can be very different from the reality with non-repeated surface landuse patterns and atmospheric variables. Therefore such periodic WRF-LES simulations are restricted to fundamental studies of the atmospheric boundary layer flow (Nunalee et al., 2014). As one step moving towards enabling WRF's capability of nesting from realistic meso-scale meteorological fields with mean flow information to micro-scale turbulent flows with additional turbulent information, we implement a well-tested synthetic turbulence inflow scheme (Xie and Castro 2008) in the WRF-LES model (v.3.6.1) at a high resolution.

Dhamankar et al. (2018) reviewed three broad classes of methods to generate the turbulent inflow conditions for LES models, mainly for engineering type of applications. The first class is the library-based method, which relies on an external turbulence library to provide inflow turbulences. The turbulence library can be based on either the precursor/concurrent simulation (e.g. Munters et al., 2016) on the same geometry (to a main LES simulation) or the pre-existing database (e.g. Schluter et al., 2004;Keating et al., 2004) from experiments or computations (on a different geometry to a main LES simulation). Although this method is not very practical (limited to specialised applications), it can provide good-quality inflow turbulence with little adjustment to inflow boundaries. The second class is the recycling-rescaling based method (e.g. Lund et al., 1998;Morgan et al., 2011), in which the velocity field is recycled from a downstream location and re-introduced back to the inlet. Although this method may be effective in producing the well-established turbulence, there are some limitations, e.g. the requirements of an equilibrium region near the inlet and a relatively larger domain. The serious limit of the first and second classes is that they only generate one shape of velocity profile determined by the geometry of the precursor simulation. The third class is the synthetic turbulence generator, which includes a variety of methods such as the Fourier transform-based method (e.g. Kraichnan, 1970;Lee et al., 1992), proper orthogonal decomposition-based method (e.g. Berkooz et al., 1993;Kerschen et al., 2005), digital filter-based method (e.g. Xie and Castro, 2008;Klein et al., 2003;Kim et al., 2013), diffusion-based method (e.g. Kempf et al., 2005), vortex method (e.g. Benhamadouche et al., 2006) and synthetic eddy method (e.g. Jarrin et al., 2006). The synthetic turbulence generator has the potential to be used for a wide range of flows. Due to the imperfection in synthetic formulation, these normally require some inputs and a certain distance for the turbulence to be well-established. For more on the above synthetic turbulence generation methods, the readers are recommended to read Tabor and Baba-Ahmadi (2010), Wu (2017) and Bercin et al. (2018).

https://doi.org/10.5194/gmd-2019-165
Preprint. Discussion started: 22 July 2019

Geoscientific Model Development Discussions

Several other methods have been developed to generate inflow turbulence for atmospheric boundary layer flow in nested WRF-LES models. Mirocha et al. (2014) introduced simple sinusoidal perturbations to the potential temperature and horizontal momentum equations near the inflow boundaries. This method can speed up the development of turbulence and generally has a satisfactory performance in the nested WRF-LES domains, providing promising results. Munoz-Esparza et al. (2014) extended the perturbation method of Mirocha et al. (2014) and proposed four methods, i.e. point perturbation method, cell perturbation method, spectral inertial subrange method and spectral production range perturbations, to generate perturbations of the potential temperature for a buffer region near the nested inflow planes. The cell perturbation method was found to have the best performance regarding the adaption distance for the fully-developed turbulence. It has the advantages of negligible computational cost, minimal parameter tuning, not requiring *a priori* turbulent information and efficiency to accelerate the development of turbulence. Munoz-Esparza et al. (2015) further generalised the cell perturbation method of Munoz-Esparza et al. (2014) under a variety of large-scale forcing conditions for the neutral atmospheric boundary layer. The perturbation Eckert number (describing the interaction between the large-scale forcing and the buoyancy contribution due to the perturbation of potential temperature) was identified as the key parameter which governs the transition to turbulent flow for nested domains. They found an optimal Eckert number for the best performance to establish a developed turbulent state under neutral atmospheric conditions. Generally speaking, these methods impose "while-noise" perturbations, thus having a flat spectrum, to a variable (e.g. temperature) at the inlet, and the model dynamics will "process" the signals once these signals are advected into the domain, e.g. to dissipate high-wavenumber signals quickly and to adjust low-wavenumber signals gradually. Strictly speaking, these methods are not inflow turbulence generation methods which are aimed at providing spatially and temporally correlated wind fields with appropriate power spectra. It is thus not surprising that a very long distance, e.g. 20 – 40 boundary layer depths, is normally required to allow a transition to fully developed turbulence. The optimisation and generalisation of these methods would also require intensive testing. Munoz-Esparza et al. (2014) commented that 'the use of temperature perturbations presents an alternative'.

Due to its accuracy, efficiency and in particular the capability for high Reynolds number follows, the synthetic inflow turbulence generator (Xie and Castro, 2008) has been implemented and tested on engineering type of codes, such as Star-CD (Xie and Castro, 2009) and OpenFOAM (Kim and Xie, 2016) and the micro-scale meteorology code PALM (PALM, 2017). This study will focus on an implementation of this synthetic inflow turbulence generator (Xie and Castro, 2008) in the idealised WRF-LES (v3.6.1) model under neutral atmospheric conditions. In this paper, Section 2 describes the methodology of WRF-LES model and the technique of the synthetic inflow turbulence generator; Section 3 presents the results of the WRF-LES model with the use of the synthetic inflow turbulence generator; and Section 4 states the conclusions and future work.

https://doi.org/10.5194/gmd-2019-165
Preprint. Discussion started: 22 July 2019

Geoscientific Model Development Discussions

2 Methodology

2.1 WRF-LES model

The atmospheric boundary layer is simulated by the compressible non-hydrostatic WRF-LES model, which computes large energy-taking resolved eddies directly and parameterises small unresolved eddies (more universal in nature) using subgrid-scale (SGS) turbulence schemes (Moeng et al., 2007). The filtered continuity and Navier-Stokes equations are (Nottrott et al., 2014):

$$\frac{\partial \tilde{u}_i}{\partial x_i} = 0, \tag{1}$$

$$\frac{\partial \tilde{u}_i}{\partial t} + \frac{\partial \tilde{u}_i \tilde{u}_j}{\partial x_j} = \upsilon \frac{\partial^2 \tilde{u}_i}{\partial x_j \partial x_j} - \frac{1}{\tilde{\rho}} \frac{\partial \tilde{p}}{\partial x_i} - \frac{\partial \tau_{ij}}{\partial x_j} + \tilde{F}_i, \tag{2}$$

where i (or j) = 1, 2, 3, represents the component of the spatial coordinate, $\tilde{u}$ is the filtered velocity, x is the spatial coordinate, t is the time, $\tilde{p}$ denotes the filtered pressure, $\tilde{\rho}$ is the filtered density, υ is the fluid kinematic viscosity, τ_{ij} are the SGS stresses, $\tilde{F}$ represents an external force term (normally involving the Coriolis force caused by the rotation of the Earth and the large-scale geostrophic forcing).

For the closure of Eq. (2), τ_{ij} are parameterised using SGS models. In this study, the 1.5-order turbulent kinetic energy (TKE) SGS model is used,

$$\tau_{ij} = -2\upsilon_{sgs}\tilde{S}_{ij}, \tag{3}$$

where $\tilde{S}_{ij}$ is the filtered strain-rate tensor and calculated as,

$$\tilde{S}_{ij} = \frac{1}{2}\left(\frac{\partial \tilde{u}_i}{\partial x_j} + \frac{\partial \tilde{u}_j}{\partial x_i}\right), \tag{4}$$

υ_{sgs} denotes the SGS eddy-viscosity and is defined as,

$$\upsilon_{sgs} = C_k \ell k_{sgs}^{1/2}, \tag{5}$$

where C_k is a model constant, ℓ is the SGS length scale and under neutral conditions, ℓ equals the grid volume of size (Δ) (Deardorff, 1970),

$$\Delta = (\Delta x\, \Delta y \Delta z)^{1/3}, \tag{6}$$

k_{sgs} is the SGS TKE with the transport equation of

$$\frac{\partial k_{sgs}}{\partial t} + \frac{\partial}{\partial x_i}\left(k_{sgs}\tilde{u}_i\right) = 2\upsilon_{sgs}\tilde{S}_{ij}\tilde{S}_{ij} + \left(\upsilon + \upsilon_{sgs}\right)\frac{\partial^2 k_{sgs}}{\partial x_i \partial x_i} - C_\varepsilon \frac{k_{sgs}^{1.5}}{\ell}, \tag{7}$$

https://doi.org/10.5194/gmd-2019-165
Preprint. Discussion started: 22 July 2019

Geoscientific Model Development Discussions

where C_ε is a model constant.

2.2 Synthetic inflow turbulence generator

The synthetic inflow turbulence generator in Xie and Castro (2008) adopted the digital filter-based method and is used in this study. For simplicity, a one-dimensional problem is used first to describe this method. The two-point velocity correlations $R_{uu}(k\Delta x)$ are assumed to be represented by an exponential function:

$$\frac{\overline{u_m u_{m+k}}}{\overline{u_m u_m}} = R_{uu}(k\Delta x) = \exp\left(-\frac{\pi|k|}{2n}\right), \tag{8}$$

where n is related to the integral length scale $L = n\Delta x$ with the grid size of Δx, u_m is the digital-filtered velocity,

$$u_m = \sum_{j=-N}^{N} b_j r_{m+j}, \tag{9}$$

where r_m is a sequence of random data with mean $\overline{r_m} = 0$ and variance $\overline{r_m r_m} = 1$, N is related to the length scale for the filter (here $N \geq 2n$), and b_j is the filter coefficient and can be estimated from

$$b_k = \tilde{b}_k / \left(\sum_{j=-N}^{N} \tilde{b}_j^2\right)^{1/2}, \text{ where } \tilde{b}_k \cong \exp\left(-\frac{\pi|k|}{n}\right). \tag{10}$$

For a two-dimensional filter coefficient, it can be obtained that

$$b_{jk} = b_j b_k, \tag{11}$$

which will then be used to filter the two-dimensional random data at each time step,

$$\varphi_m(t, x_j, x_k) = \sum_{j=-N_j}^{N_j} \sum_{k=-N_k}^{N_k} b_{jk} r_{m+j,m+k}, \tag{12}$$

where m indicates the velocity component. At the next time step, the filtered velocity field is calculated as,

$$\Psi_m(t + \Delta t, x_j, x_k) = \Psi_m(t, x_j, x_k) \exp\left(-\frac{\pi\Delta t}{2T}\right) + \varphi_m(t, x_j, x_k)\left[1 - \exp\left(-\frac{\pi\Delta t}{T}\right)\right]^{0.5}, \tag{13}$$

where T is the Lagrangian time scale representing the persistence of the turbulence, $\varphi_m(t, x_j, x_k)$ is calculated based on Eq. (12). Xie and Castro (2008) demonstrated that Eq. (13) satisfies the correlation functions in an exponential form in space and in time. In contrast to three-dimensional filter, the two-dimensional filter in Xie and Castro (2008) is more computationally efficient.

Finally, the velocity field is obtained by using the simplified transformation proposed by Lund et al. (1998),

$$\tilde{u}_i = \bar{u}_i + \alpha_{ij}\Psi_j, \tag{14}$$

where

$$\alpha_{ij} = \begin{bmatrix} (\tilde{R}_{11})^{1/2} & 0 & 0 \\ \tilde{R}_{21}/\alpha_{11} & (\tilde{R}_{22} - (\alpha_{21})^2)^{1/2} & 0 \\ \tilde{R}_{31}/\alpha_{11} & (\tilde{R}_{32} - \alpha_{21}\alpha_{31})/\alpha_{22} & (\tilde{R}_{33} - (\alpha_{31})^2 - (\alpha_{32})^2)^{1/2} \end{bmatrix}, \tag{15}$$

https://doi.org/10.5194/gmd-2019-165
Preprint. Discussion started: 22 July 2019


Geoscientific Model Development Discussions

and $\tilde{R}_{ij}$ is the resolved Reynolds stress tensor, which can be estimated based on measurements or other simulations with periodic boundary conditions.

2.3 Model coupling and configuration

In this study, we firstly configured a WRF-LES model with periodic boundary conditions in both streamwise and lateral directions to obtain *a priori* turbulent information, such as the vertical profiles of mean velocity and dominant Reynolds stress tensors, which are required by the synthetic inflow turbulence generator. The integral length scales in the *x*, *y* and *z* directions are specified based on relative ratios to the boundary layer height (i.e. 500 m in this study shown as Fig. **1**a for LS1.0), similar to that in Xie and Castro (2008). The streamwise length scale (L_x) is specified based on the mean streamwise velocity profile and a constant Lagrangian time scale *T* (Eq. 13) using Taylor's hypothesis. The lateral length scale (L_y) is specified a constant value. The vertical length scale (L_z) is specified a smaller constant value near the bottom (close to canopy height) and a larger constant value for the upper domain, explained in Xie and Castro (2008). A sensitivity study of integral length scales (for the three L_x, L_y *and* L_z) with ratios of (0.6, 0.8, 1.2, and 1.4) is also conducted. The size of the computational domain is 9.98 km×2.54 km×0.5 km (in *x*, *y* and *z* directions), with the resolutions of $\Delta x = \Delta y = 20\ m$ and stretched Δz (from about 3 m up to 27 m). The grid number is then 499×127×49. In order to achieve the vertically same wind direction, the Coriolis force is turned off in this study and a constant pressure gradient force is specified as the external driving force in Eq. (2), similar to that used in Ma and Liu (2017), resulting in a prevailing wind speed of about 10 m s^{-1} at the domain top.

For the cases with the synthetic inflow turbulence at the inlet and periodic conditions in the lateral direction, the constant pressure gradient force is not necessary anymore; instead, a pressure-drop between the inlet and outlet is implicitly derived from the prescribed mean momentum profiles as part of the synthetic inflow and the outflow boundary conditions in the solver. The periodic case is used for the validation of the results from the inflow case. The WRF-LES is solved at a time step of 0.2 s. A spin-up period 6 h is adopted for the inflow cases to allow the synthetic inflow turbulence to fully develop in the WRF-LES model. The further 1 h output with 1 minute interval is used for the analysis. In this study, as the turbulent flow is laterally homogeneous, we take advantage of averaging both in lateral direction and in time for the calculation of the vertical profiles of statistical data (Ghannam et al., 2015).

In the synthetic inflow turbulence generator, a uniform mesh is used with resolutions of $\Delta y = 20\ m$ (same as that on the physical inlet of the WRF-LES domain) and $\Delta z = 4.2\ m$ (slightly larger than the smallest vertical grid spacing of the WRF-LES domain). The filtered three velocity components at the inlet from the inflow generator are then interpolated onto the vertically non-uniform mesh in the WRF-LES domain. The standalone synthetic turbulence generator code in Xie and Castro (2008) is originally run on a single processor, whereas the WRF-LES simulation is run in parallel mode. It is necessary to

https://doi.org/10.5194/gmd-2019-165
Preprint. Discussion started: 22 July 2019


Geoscientific Model Development Discussions

ensure that each processor in the parallel mode has the same information of the 2-dimensional slice of flow field before each processor can extract the corresponding patch from the same 2-dimensional inlet data. In this implementation, the synthetic turbulence generator code is firstly run on the master processor at each WRF-LES time step. The generated inlet data are then passed to other processors. The flow field at the inlet of each corresponding processor would be then updated at every time step accordingly. The computation time for a typical WRF-LES time step between the periodic case and the inflow cases is compared in Fig. 1(b). The computation time for the inflow case LS1.0 is nearly double of the periodic case, mostly indicating the additional computational time associated with the synthetic inflow turbulence generator and data passing. It is not surprising that the computation time increases with the increase in the integral length scale since bigger arrays are constructed and computed for the filter velocity in the synthetic inflow turbulence generator as in Eq. (9) for the larger integral length scale.

3 Results

3.1 BASE case output

3.1.1 Horizontal slices of instantaneous velocity components

Fig. 2 illustrates the horizontal slices of instantaneous streamwise (Figs. 2a and 2b) and vertical (Figs. 2c and 2d) velocity components at $z/H = 0.1$ in the periodic case and the inflow case (LS1.0 in Fig. 1a) while the turbulence flow is established after 5 hours simulation time. The synthetic turbulence structures imposed at the inlet are advected and decay downwind the domain, and are adjusted by the model dynamics at further downwind distances. After a short adjustment distance, the inflow case clearly generates turbulence streaks, which are similar to these in the periodic case. Other quantities that may further demonstrate this adjustment distance will be discussed in the following subsections. This suggests that the synthetic inflow turbulence generator can generate realistic well-configured turbulence structures from a short adjustment distance downwind. For the periodic case, the turbulence structures are recycled from the outlet to the inlet of the domain, and there is no adjustment distance, and instead, an adjustment time to generate fully-developed turbulence structures.

3.1.2 Development of local friction velocity

Fig. 3 shows the development of laterally and temporally averaged local friction velocity in the periodic case and the inflow case (LS1.0), where $\hat{u}_*$ is the local friction velocity along the streamwise direction normalised by the global u_* for the whole domain. The variation of the local friction velocity is within ±1% u_* along the streamwise direction for the periodic case and is within about ±1.5 % u_* after a downwind distance of $x/H = 5$ for the inflow case. There is a larger variation close to the inlet region ($x/H < 5$) for the inflow case. This is because the imposed turbulence on the inflow plan is 'synthetic', which develops in a short distance in the WRF-LES solver.

https://doi.org/10.5194/gmd-2019-165
Preprint. Discussion started: 22 July 2019

Geoscientific Model Development Discussions

3.1.3 Horizontal profiles of mean flow and turbulence quantities

Fig. 4 illustrates laterally and temporally averaged horizontal profiles of (a) $< u >/u_*$, (b) $< u'^2 >/u_*^2$, (c)$< v'^2 >/u_*^2$, (d) $< w'^2 >/u_*^2$, (e) $< u'w' >/u_*^2$ and (f) $< TKE >/u_*^2$ at $z/H = 0.1$ and $z/H = 0.5$ for the periodic case and the inflow case (LS1.0). These horizontal profiles show the development of synthetic turbulence generated by the inflow generator. There are only slight differences in $<u >/u_*$ between the periodic case and the inflow case. This suggests that the inflow case reproduces successfully the desired mean wind profile. The curves of $< u'^2 >/u_*^2$ for both cases match well with each other at $x/H = 5$, although there is a sudden jump close to the inlet and a subsequent decrease until the location of convergence. $< u'^2 >/u_*^2$ has a higher value at $z/H = 0.1$ than that at $z/H = 0.5$. This is consistent with the trend that it decreases with height in the boundary layer. The other two normal stresses $<v'^2 >/u_*^2$ and $< w'^2 >/u_*^2$ have the same behaviour. The horizontal profile of $<v'^2 >/u_*^2$ for the inflow case is in a good agreement against that for the periodic case in the entire domain. The development of $< w'^2 >/u_*^2$ in the streamwise direction at $z/H = 0.5$ is achieved at about $x/H = 6$, whereas that at $z/H = 0.1$ takes much longer to be achieved. The time scale of the development of $< u'w' >/u_*^2$ and TKE/u_*^2 is similar to that of $< u'^2 >/u_*^2$. This can be explained by the fact that the streamwise velocity fluctuations have a major contribution to $< u'w' >$ and TKE. The slower adjustment of *TKE* at $z/H = 0.1$ (closer to the ground) than that at $z/H = 0.5$ (the middle of the boundary layer) can be attributed to a larger shear-generated TKE there together with a downward turbulence transport from above.

3.1.4 Vertical profiles of mean flow and turbulence quantities

Fig. 5 shows the laterally and temporally averaged vertical profiles of (a) $< u >/u_*$, (b) $< u'^2 >/u_*^2$, (c) $< v'^2 >/u_*^2$, (d) $< w'^2 >/u_*^2$, (e) $< u'w' >/u_*^2$ and (f) $< TKE >/u_*^2$ at a series of downwind locations, $x/H = 2$, 4, 6 and 10, for the inflow case (LS1.0). The red circle dots in Fig. 5 are the spatially (including both in the streamwise and lateral directions) and temporally averaged vertical profiles for the periodic case. It is noticed again that these data for the periodic case are also used as the inputs for *a priori* turbulence information required by the synthetic inflow turbulence generator. $< u >/u_*$ profiles of the inflow case match closely to that of the periodic case. This suggests that the inflow case achieves the desired the mean wind profile given that the sampled data are limited. $< u'^2 >/u_*^2$ converges towards the periodic profile after $x/H = 6$ as shown in Fig. 5 (b). Although $< v'^2 >/u_*^2$, $< w'^2 >/u_*^2$ and $< TKE >/u_*^2$ vertical profiles in the inflow case show small variations between different locations, they are all in a good agreement with the data of the periodic case. These are consistent with the results shown in Fig. 4. The Reynolds shear stress $< u'w' >$, which is the cross correlation between the streamwise and vertical velocity fluctuations, usually converges slower than the normal Reynolds stresses, e.g. $< v'^2 >$. Overall, the synthetic inflow turbulence generator performs well in terms of the development of the mean flow and the turbulence quantities against the data from the periodic case.

https://doi.org/10.5194/gmd-2019-165
Preprint. Discussion started: 22 July 2019

Geoscientific Model Development Discussions

3.1.5 Spectra analysis

Fig. 6 illustrates the spectra of the streamwise wind component at a series of downwind locations ($x/H = 2, 4, 6,$ and 10) at $z/H = 0.5$ for the periodic case and the inflow case (LS1.0). For each *x*-location, e.g. $x/H = 2$, the spectrum for the inflow case was firstly calculated from the streamwise wind component over lateral direction (y_j) for a given time t_n, namely, $\tilde{u}(t_n, 2H, y_j, 0.5H)$, and then an average over time t_n yields the data plotted in Fig. **6**. The spectrum for the periodic case is calculated using the same method as that for the spectra in the inflow case, with an additional average over the streamwise direction, x. There is evidence of the tendency in the profiles from the inlet downstream to recover closely to that of the periodic case. The spectrum decreases slightly with the increase of the downwind distance at the high wavenumbers, suggesting a decay of small eddies when the synthetic turbulence is advected downwind. The spectrum in Munoz-Esparza et al. (2015) drops much steeper at the high wavenumbers (noticing that their plots were for kE_{u_i} with the inertial subrange of -2/3 slope and the numerical dissipation slope of about -9), whereas in our simulations the spectra drops more gently at the high wavenumbers (our plots are for E_u with the inertial subrange of -5/3 slope and the numerical dissipation slope of about -5). This is partially attributed to the fact that our resolution of 20 m in the horizontal direction is much finer than their resolution of 90 m. Note Munoz-Esparza et al. (2015) also compared the stochastic perturbation method with those obtained using Xie and Castro (2008). Our current results generated in WRF-LES are consistent with those in Munoz-Esparza et al. (2015). This also confirms that synthetic turbulence with an inertial sublayer in the spectrum generated by using Xie and Castro (2008) method is able to sustained in WRF-LES for a very high resolution.

3.2 Sensitivity tests of integral length scale in the flow cases

It is not trivial to optimise the integral length scales of the inlet turbulence generator. Therefore, it is necessary to conduct sensitivity tests of the integral length scales. Fig. **7** shows the influence of integral length scale on the development of local friction velocity. A length scale (LS) ratio from 0.6 to 1.4 to those in the LS1.0 case are tested. For all inflow cases, there is a sudden change near the inlet due to the imposed inflow turbulence. The adjustment distance to well-established turbulence is shorter for the case with the smaller integral length scale, i.e. about $x/H = 2$ for the cases LS0.6-0.8, and about $x/H = 5$ for the cases of LS1.0-1.4. This suggests that the imposed integral length scales for the inflow turbulence slightly affect the convergence to well-developed turbulence. It is also observed that a variation of ±40% in the integral length scales in the cases LS0.6-1.4 yields a variation of less than 2% in the local friction velocity. This suggests that the sensitivity of the tested integral length scales on the local friction velocity is not significant in the WRF-LES model, which is consistent with that in engineering type CFD solvers in Xie and Castro (2008).

Fig. 8 shows effects of integral length scale on the horizontal profiles of (a) $< u >/u_*$, (b) $<u'^2>/u_*^2$, (c)$< v'^2 >/u_*^2$, (d) $< w'^2 >/u_*^2$, (e) $< u'w' >/u_*^2$ and (f) $<TKE>/u_*^2$ at $z/H = 0.5$. Fig. 8 (a) shows that $< u >/u_*$ is slightly greater for the LS ratio less 1.0 (see Fig. 8a for comparison). This is due to a greater Reynolds shear stress $< u'w' >/u_*^2$ shown in Fig. 8

https://doi.org/10.5194/gmd-2019-165
Preprint. Discussion started: 22 July 2019

Geoscientific Model Development Discussions

(e). Fig. 8 (b-d) and (f) show that in general the normal stresses $<u'^2>/u_*^2$, (c)$<v'^2>/u_*^2$, (d) $<w'^2>/u_*^2$ and the $<TKE>/u_*^2$ increase as the LS ratio increases. This is because small eddies tend to decay faster than large eddies. It is crucial to note that for those with the integral length scales close to the 'accurate' ones, i.e. LE ratio equal to one, the development distance to converged turbulence is shorter compared to other cases. Fig. 9 shows effects of integral length scale on vertical profiles at typical streamwise locations of the mean velocity, Reynolds stresses and TKE, confirms the findings suggested from Fig. 8.

Fig. 10 shows the effect of the integral length scale on the spectra of the streamwise veloicty component at $x/H = 10$ and $z/H = 0.5$. There is no significant change of the spectra with the change in the integral length scale considered in the current study. A very small variation of the spectra is within the uncertainty of the calculation of spectrum from the raw data.

4 Discussion and conclusions

A synthetic inflow turbulence generator (Xie and Castro, 2008) was implemented in idealised WRF-LES (v3.6.1) models under neutral atmospheric conditions. A WRF-LES model with periodic boundary conditions was firstly configured to provide *a priori* turbulence statistical data for the synthetic inflow turbulence generator. The integral length scales were estimated at appropriate ratios to the boundary layer height as in (Xie and Castro, 2008). The results from the inflow cases were then compared with those from the periodic case. It is not trivial to estimate the integral length scales as the primary input of the inflow turbulence generator. Therefore sensitivity tests of integral length scales on the wall shear stress, the mean flow, the Reynolds shear stresses and the turbulence spectra for the flow cases were conducted.

The inflow case with the baseline integral length scales generates similar turbulence structures to those for the periodic case after a short adjustment distance. The WRF-LES model with the inflow generator reproduces realistic features of turbulence in the neutral atmospheric boundary layer. The development of local friction velocity suggests that a downwind distance of 5 boundary layer heights is required to recover the local friction force for the inflow case with an error of about ±1.5% u_*. This is consistent with that in in Xie and Castro (2008) and Kim et al (2013). Keating et al. (2004) suggested a development distance of about 20 half-channel depth for modelling a plane channel flow and this may be owing to the different synthetic turbulence generation approaches they adopted. Laraufie et al. (2011) suggested that an increase in the Reynolds number decreases the adjustment distance when a synthetic inflow turbulence generator is used. For our case of the atmospheric boundary layer here, the Reynolds number is extremely large and thus adopting synthetic inflow turbulence generator for the atmospheric boundary layer should be advantageous to that for an engineering flow.

Horizontal and vertical profiles of mean velocity and turbulence second moment statistics further confirm that a very short distance is required for the development of synthetic turbulence. The mean velocity profiles at all tested locations in the

https://doi.org/10.5194/gmd-2019-165
Preprint. Discussion started: 22 July 2019


Geoscientific Model Development Discussions

domain were close to the desired profiles, while the turbulence second moment statistics profiles were in reasonable agreement with the desired profiles about $x/H = 5 - 10$ downwind of the inlet. The adjustment distances of turbulence second moment statistics are crucial for the assessment of the synthetic inflow turbulence generator. Reducing the integral length scales can shorten the adjustment distance. We found that the influence of integral length scale on the mean velocity profiles is insignificant, whereas such an influence on the turbulence second moment statistics is more noticeable. It would require the additional computational time in the synthetic inflow turbulence generator compared with the period case. This will be certainly improved by running the synthetic inflow generation subroutine in parallel as a future task.

In summary, the synthetic inflow turbulence generator is implemented successfully into the idealised WRF-LES model. The generated two-dimensional slices of data are correlated both in space and in time in the exponential form. The spectrum of these data shows an inertial subrange, and this again suggests the capability of the method for high Reynolds number flows. These tests on WRF also confirm that this method yields a satisfactory accuracy. The WRF-LES model with the synthetic turbulence generator has provided promising results as evaluated against the period case. The limitation of this method is the requirement of *a priori* turbulence statistic data and integral length scales, which can be estimated by the similarity theory of the atmospheric boundary layer or experimental data. Sensitivity studies have been performed to address this issue, in particular in terms of effect of the integral length scale. We conclude that within a certain range of the integral length scale, the numerical results are not significantly sensitive. The implementation of the synthetic inflow turbulence generator (Xie and Castro, 2008) can be extended to the WRF-LES simulation of a horizontally inhomogeneous case with non-repeated surface land-use pattern, and be further developed for the multi-scale seamless nesting case from a meso-scale domain with a km-resolution down to LES domains with metre resolutions.

Code and data availability.

The standard version of WRF v3.6.1 is available at http://www2.mmm.ucar.edu/wrf/users/download/get_sources.html. The coupling WRF v3.6.1 code with the synthetic inflow turbulence generator and case settings are archived on Zenodo (https://doi.org/10.5281/zenodo.3296011).

Author contributions.

The study was conceived by XC and ZX; JZ implemented the synthetic inflow turbulence generator code (from ZX) to the WRF-LES model (v3.6.1) and ran model simulations; all authors contributed to writing the manuscript.

Competing interests.

The authors declare that they have no conflict of interest.

Acknowledgements.

https://doi.org/10.5194/gmd-2019-165
Preprint. Discussion started: 22 July 2019

This work is part of the CityFlocks project, sponsored by the UK Natural Environment Research Council (NERC: NE/N003195/1). This work used the ARCHER UK National Supercomputing Service (http://www.archer.ac.uk).

https://doi.org/10.5194/gmd-2019-165
Preprint. Discussion started: 22 July 2019

Geoscientific Model Development Discussions

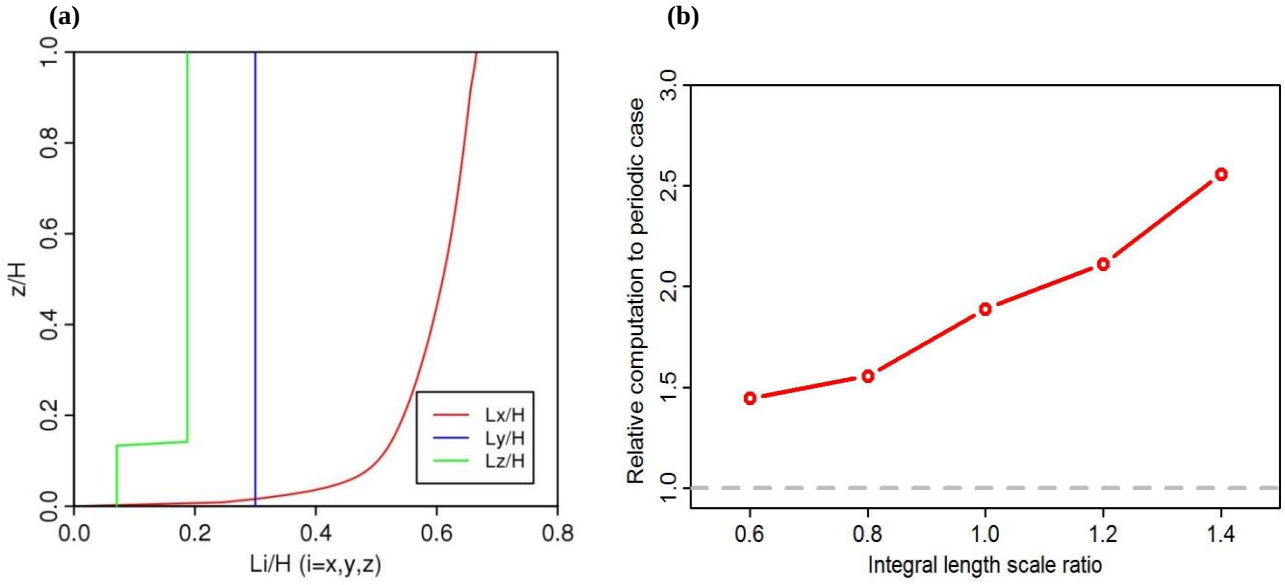

Figure 1: (a) Integral length scales prescribed at the inlet used in the inflow BASE case (LS1.0); (b) Relative computation of inflow cases to periodic case for a typical WRF-LES time step, dashed grey line of 1.0 indicating the periodic case.

https://doi.org/10.5194/gmd-2019-165
Preprint. Discussion started: 22 July 2019

Geoscientific Model Development Discussions

(a) u (m s^{-1}) for the fully periodic case

(b) u (m s^{-1}) for synthetic inflow case

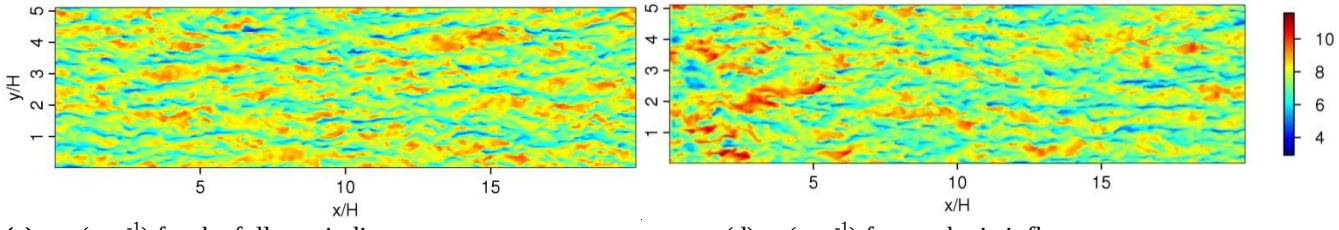

(c) w (m s^{-1}) for the fully periodic case

(d) w (m s^{-1}) for synthetic inflow case

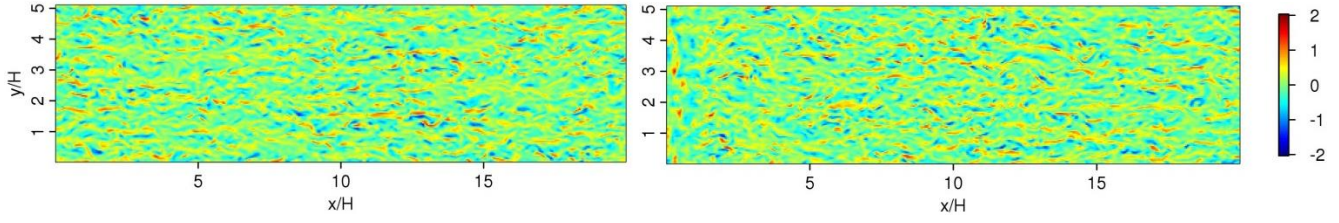

Figure 2: Horizontal slice of instantaneous velocity components at *z/H*=0.1, (a) The fully periodic case, and (b) The synthetic based inflow case while the turbulence flow is established after 5 hours simulation time.

https://doi.org/10.5194/gmd-2019-165
Preprint. Discussion started: 22 July 2019

Geoscientific Model Development Discussions

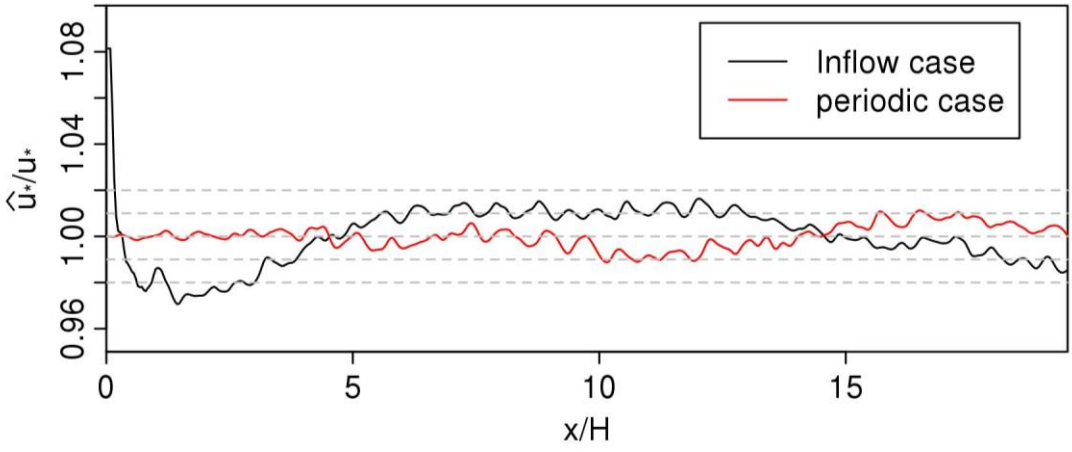

Figure 3: Development of local friction velocity (laterally and temporally) in the periodic case and the inflow case (LS1.0), with $\widehat{\boldsymbol{u}}_*$ indicating the local friction velocity along the streamwise direction normalised by the global friction velocity $\boldsymbol{u}_*$ for the whole domain.

https://doi.org/10.5194/gmd-2019-165
Preprint. Discussion started: 22 July 2019

Geoscientific Model Development Discussions

(a) $< u >/u_*$ (b) $< u'^2 >/u_*^2$

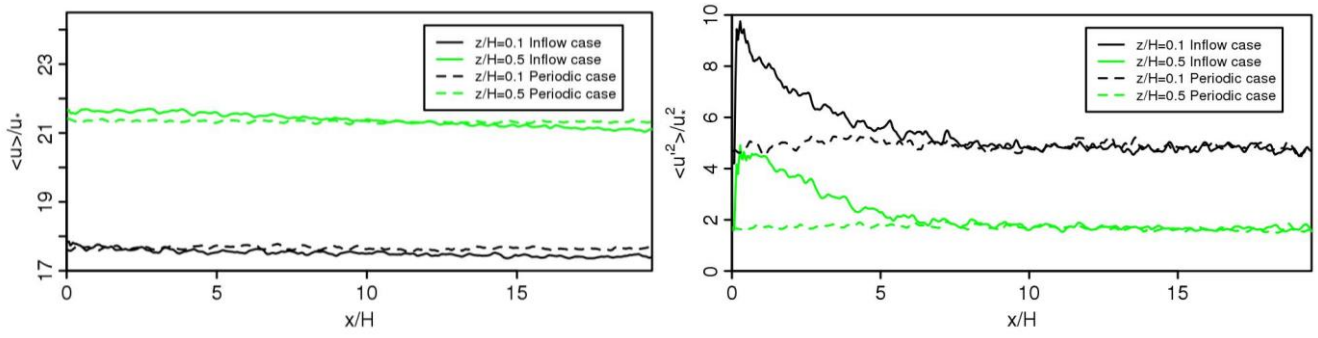

(c) $< v'^2 >/u_*^2$ (d)$< w'^2 >/u_*^2$

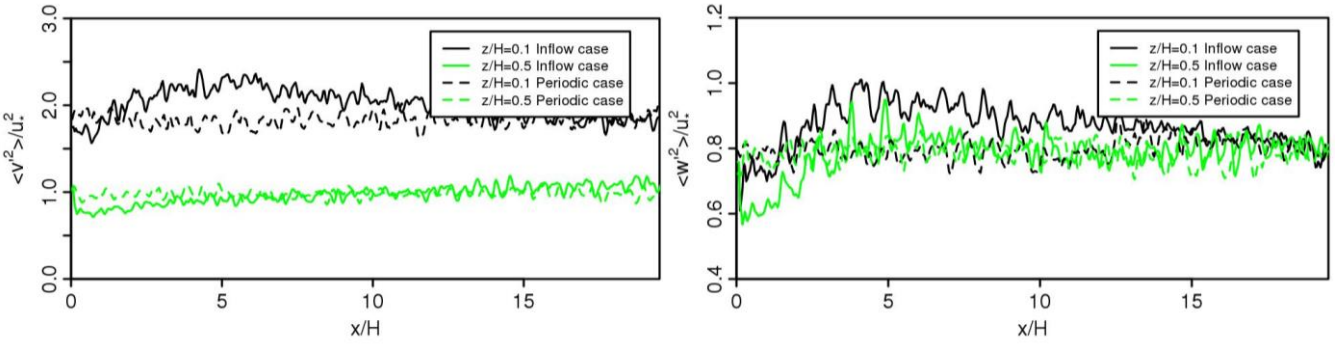

(e) $< u'w' >/u_*^2$ (f) $< TKE >/u_*^2$

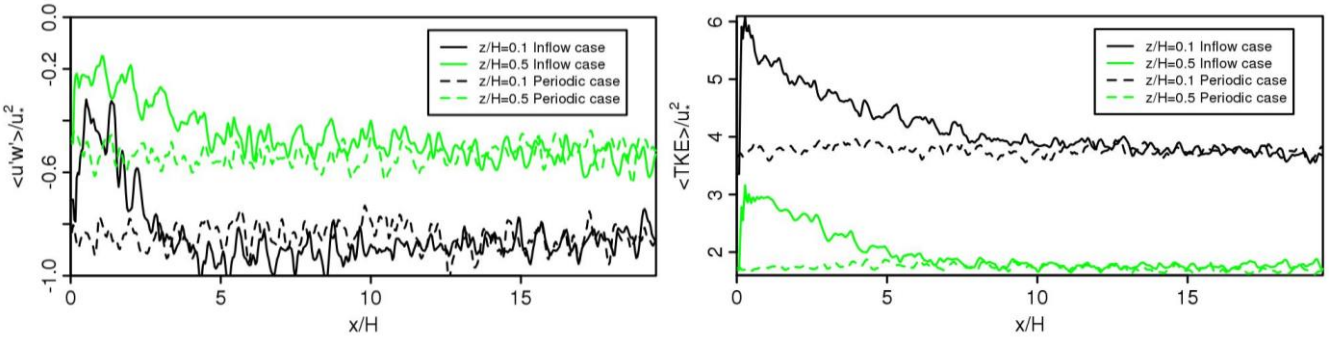

Figure 4: Horizontal profiles (spatially and temporally averaged) of (a) $< \boldsymbol{u} >/\boldsymbol{u}_*$, (b) $< \boldsymbol{u'^2} >/\boldsymbol{u}_*^2$, (c)$< \boldsymbol{v'^2} >/\boldsymbol{u}_*^2$, (d)$< \boldsymbol{w'^2} >/\boldsymbol{u}_*^2$, (e) $< \boldsymbol{u'w'} >/\boldsymbol{u}_*^2$ and (f) $< \boldsymbol{TKE} >/\boldsymbol{u}_*^2$ at *z/H*=0.1 and *z/H*=0.5 in the periodic case and the inflow case (LS1.0).

https://doi.org/10.5194/gmd-2019-165
Preprint. Discussion started: 22 July 2019

Geoscientific Model Development Discussions

(a) $< u >/u_*$ (b) $< u'^2 >/u_*^2$ (c) $< v'^2 >/u_*^2$

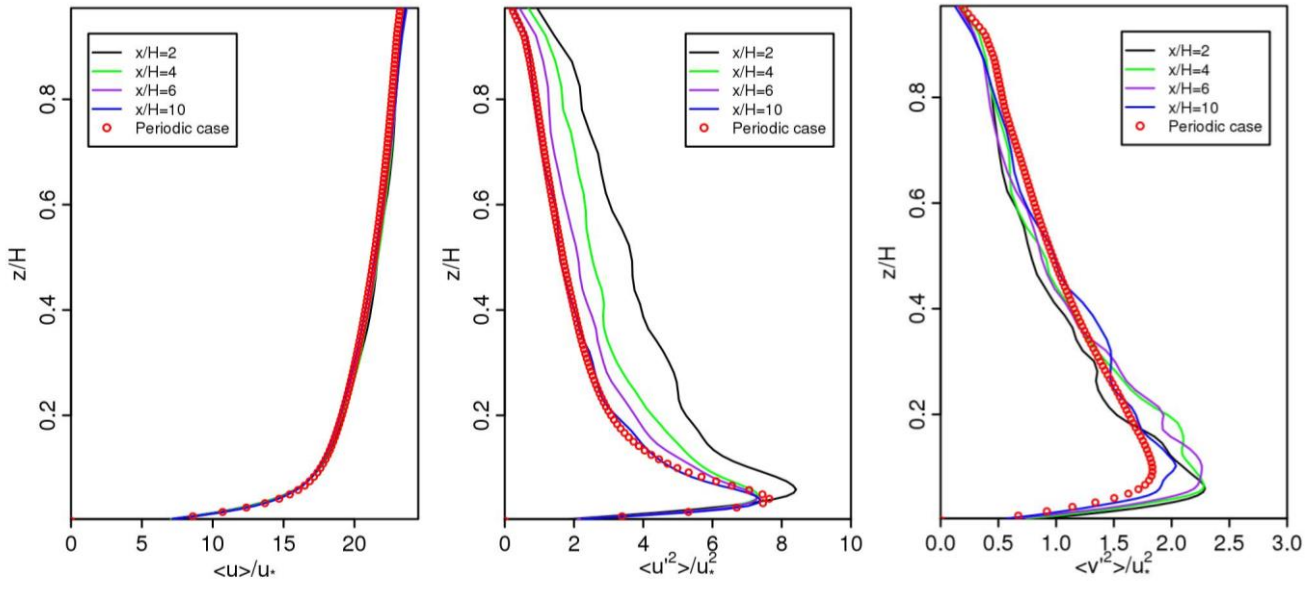

(d) $< w'^2 >/u_*^2$ (e) $< u'w' >/u_*^2$ (f) $< TKE >/u_*^2$

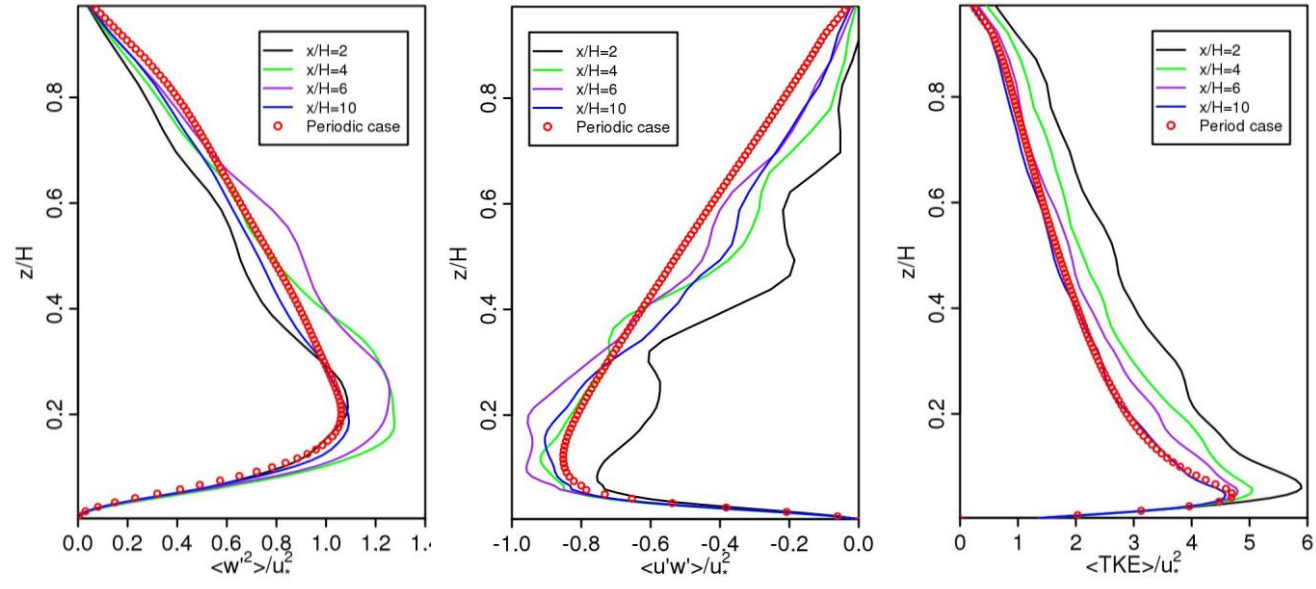

Figure 5: Laterally and temporally averaged vertical profiles of (a) $< \boldsymbol{u} >/\boldsymbol{u}_*$, (b) $<\boldsymbol{u}'^2 >/\boldsymbol{u}_*^2$, (c) $< \boldsymbol{v}'^2 >/\boldsymbol{u}_*^2$, (d) $< \boldsymbol{w}'^2 >/\boldsymbol{u}_*^2$, (e) $< \boldsymbol{u}'\boldsymbol{w}' >/\boldsymbol{u}_*^2$ and (f) $< \boldsymbol{TKE} >/\boldsymbol{u}_*^2$ at a series of downwind locations in the inflow case (LS1.0), and the periodic case (also averaged in the streamwise direction).

https://doi.org/10.5194/gmd-2019-165
Preprint. Discussion started: 22 July 2019

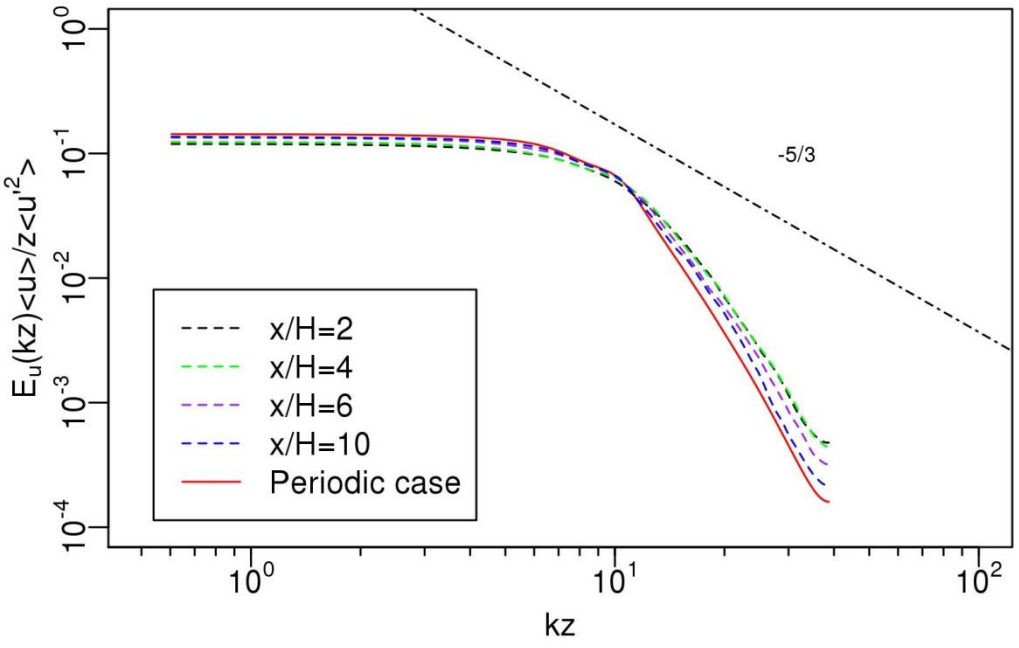

Figure 6: Spectra of streamwise wind component for a series of downwind locations at the height of z/H=0.5, k is the angular wavenumber, with $< \boldsymbol{u} >$ and $< \boldsymbol{u}' >$ the laterally averaged mean and streamwise normal Reynolds stress, respectively.

https://doi.org/10.5194/gmd-2019-165
Preprint. Discussion started: 22 July 2019

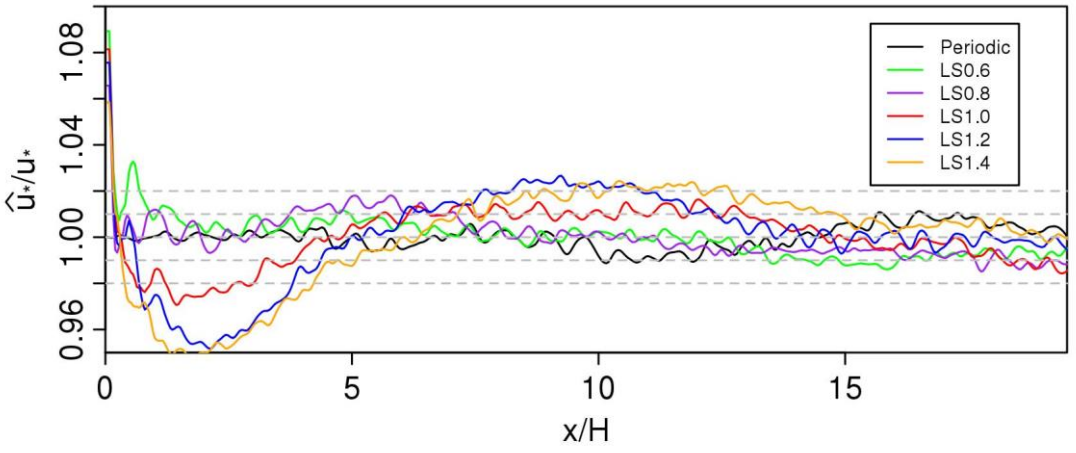

Figure 7: Development of local friction velocity (laterally and temporally) with various integral length scales. $\hat{\boldsymbol{u}}_*$ is the local friction velocity along the streamwise direction, and $\boldsymbol{u}_*$ is the global friction velocity of the whole domain.

https://doi.org/10.5194/gmd-2019-165
Preprint. Discussion started: 22 July 2019

Geoscientific Model Development Discussions

(a) $< u >/u_*$ (b) $< u'^2 >/u_*^2$

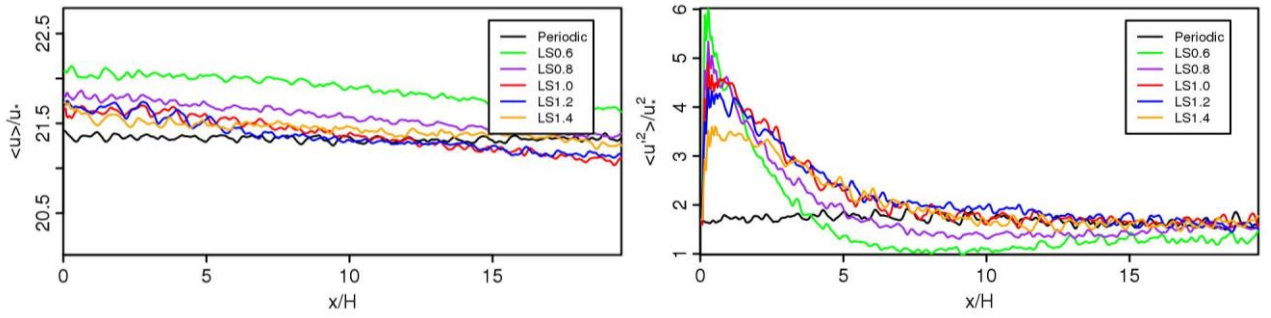

(c) $< v'^2 >/u_*^2$ (d)$< w'^2 >/u_*^2$

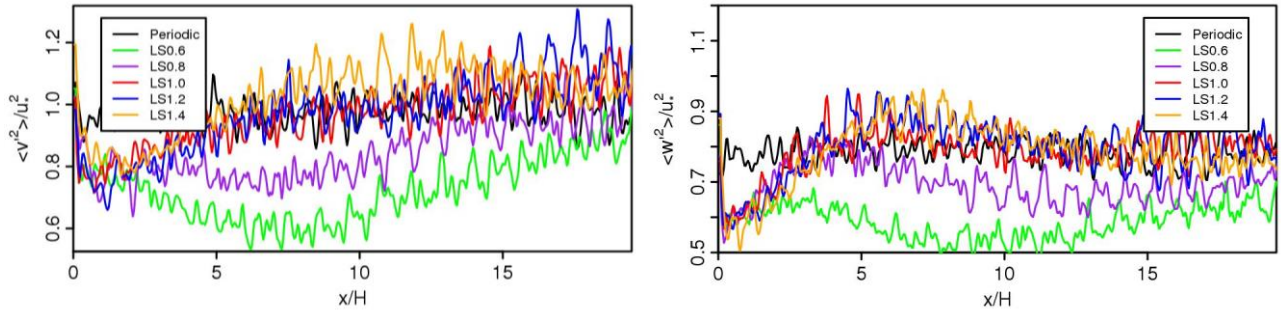

(e) $<u'w' >/u_*^2$ (f) $< TKE >/u_*^2$

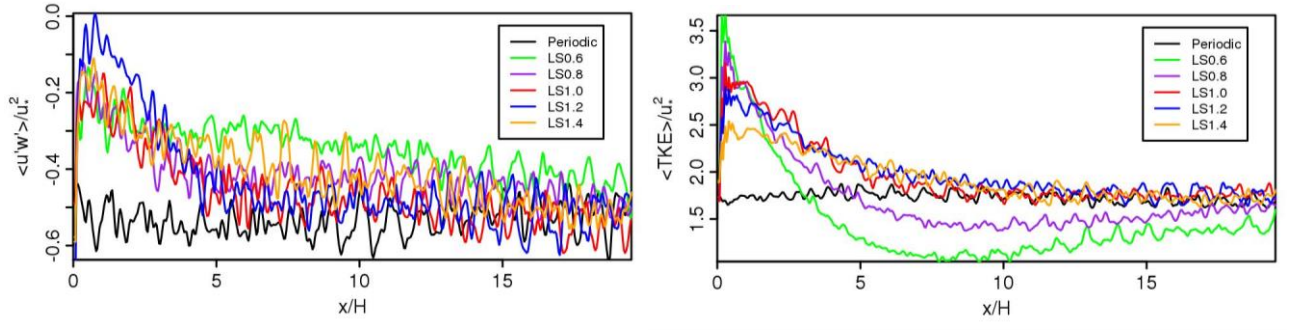

Figure 8: Horizontal profiles (spatially and temporally averaged) of (a) $< \boldsymbol{u} >/\boldsymbol{u}_*$, (b) $<\boldsymbol{u}'^2 >/\boldsymbol{u}_*^2$, (c) $< \boldsymbol{v}'^2 >/\boldsymbol{u}_*^2$, (d) $< \boldsymbol{w}'^2 >/\boldsymbol{u}_*^2$, (e) $< \boldsymbol{u}'\boldsymbol{w}' >/\boldsymbol{u}_*^2$ and (f) $< \boldsymbol{TKE} >/\boldsymbol{u}_*^2$ at *z*/*H*=0.5 with various integral length scales.

https://doi.org/10.5194/gmd-2019-165
Preprint. Discussion started: 22 July 2019

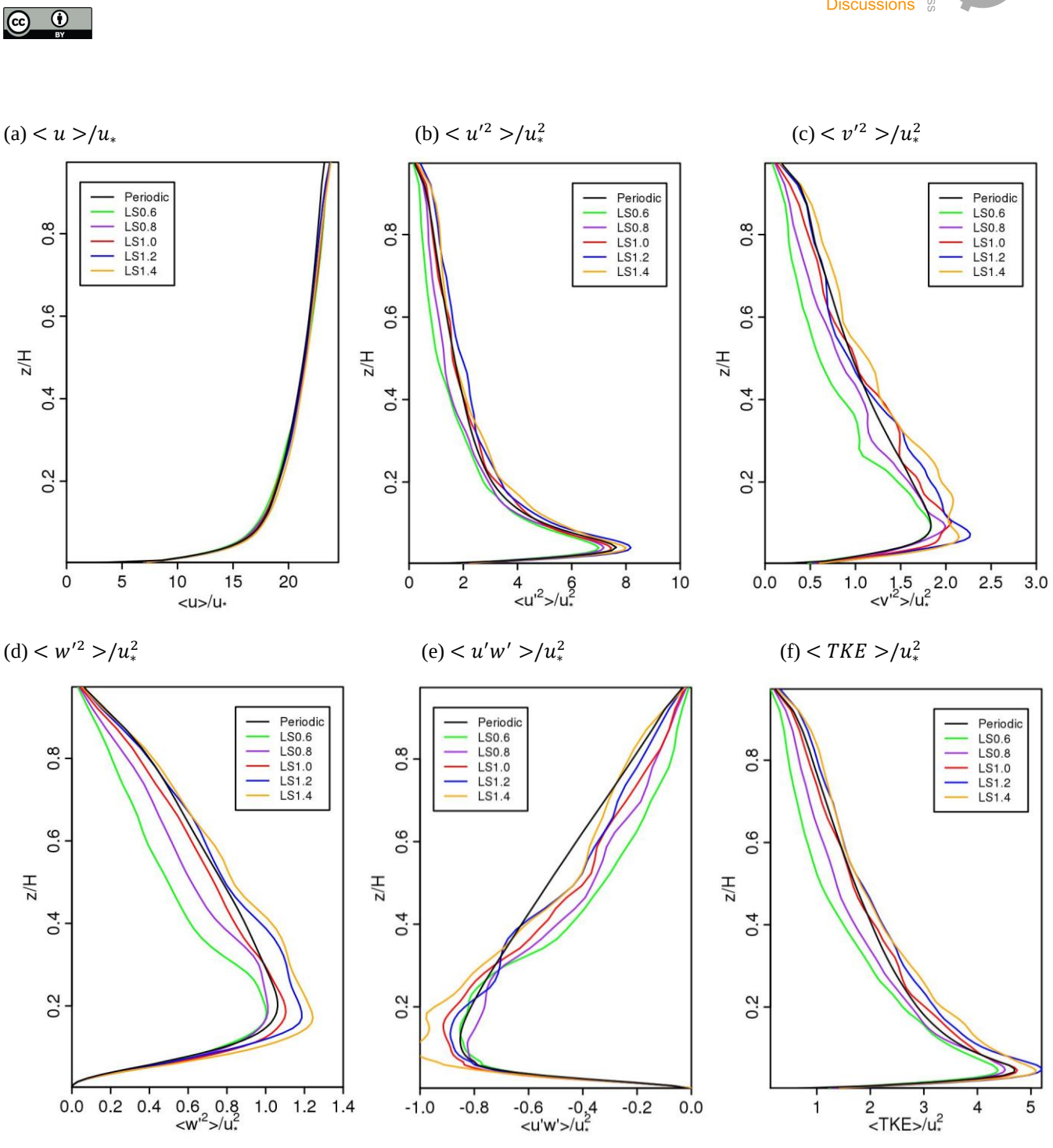

Figure 9: Vertical profiles (laterally and temporally averaged) of (a) $< \boldsymbol{u} >/\boldsymbol{u}_*$, (b) $< \boldsymbol{u}'^2 >/\boldsymbol{u}_*^2$, (c) $< \boldsymbol{v}'^2 >/\boldsymbol{u}_*^2$, (d) $< \boldsymbol{w}'^2 >/\boldsymbol{u}_*^2$, (e) $< \boldsymbol{u}'\boldsymbol{w}' >/\boldsymbol{u}_*^2$ and (f) $< \boldsymbol{TKE} >/\boldsymbol{u}_*^2$ at *x/H*=10 with various integral length scales.

https://doi.org/10.5194/gmd-2019-165
Preprint. Discussion started: 22 July 2019

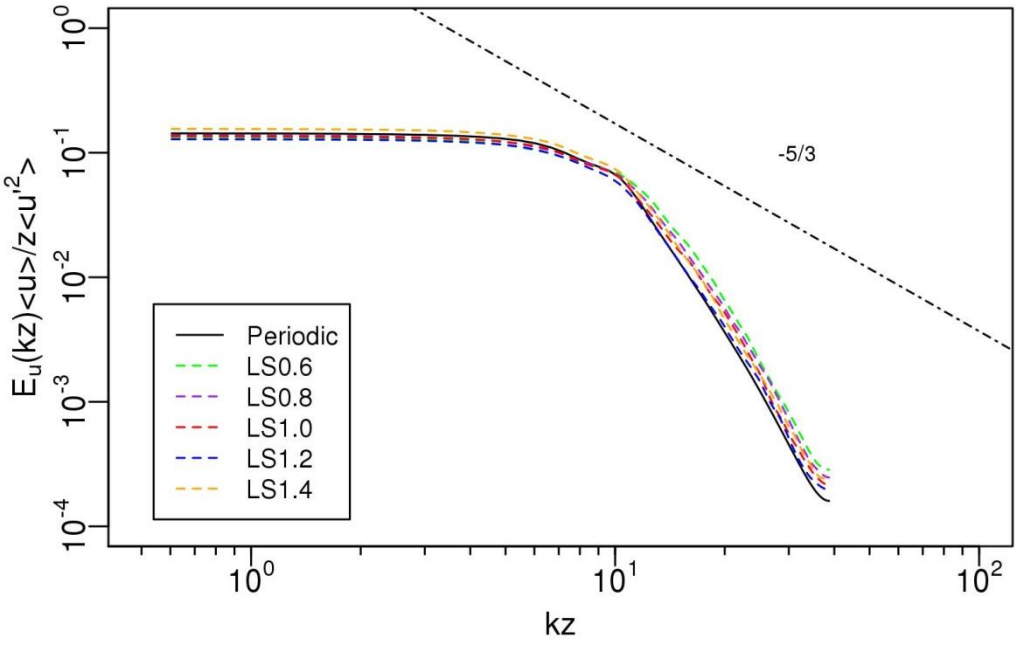

Figure 10: Spectra of streamwise wind component for a series of downwind locations at *x/H*=10 and *z/H*=0.5 with various integral length scales, k is the angular wavenumber, with $< \boldsymbol{u} >$ and $< \boldsymbol{u}^{'2} >$ the laterally averaged mean and streamwise normal Reynolds stress, respectively.

https://doi.org/10.5194/gmd-2019-165
Preprint. Discussion started: 22 July 2019

Geoscientific Model Development Discussions

References

Benhamadouche, S., Jarrin, N., Addad, Y., and Laurence, D.: Synthetic turbulent inflow conditions based on a vortex method for large-eddy simulation, Progress in Computational Fluid Dynamics, 6, 50-57, 10.1504/pcfd.2006.009482, 2006.

Bercin, K. M., Xie, Z. T., and Turnock, S. R.: Exploration of digital-filter and forward-stepwise synthetic turbulence generators and an improvement for their skewness-kurtosis, Computers & Fluids, 172, 443-466, 10.1016/j.compfluid.2018.03.070, 2018.

Berkooz, G., Holmes, P., and Lumley, J. L.: The proper orthogonal decomposition in the analysis of turbulent flows, Annual Review of Fluid Mechanics, 25, 539-575, 10.1146/annurev.fl.25.010193.002543, 1993.

Deardorff, J. W.: A numerical study of three-dimensional turbulent channel flow at large Reynolds numbers, Journal of Fluid Mechanics, 41, 453-480, 10.1017/s0022112070000691, 1970.

Dhamankar, N. S., Blaisdell, G. A., and Lyrintzis, A. S.: Overview of Turbulent Inflow Boundary Conditions for Large-Eddy Simulations, Aiaa Journal, 56, 1317-1334, 10.2514/1.j055528, 2018.

Doubrawa, P., Montornès, A., Barthelmie, R. J., Pryor, S. C., and Casso, P.: Analysis of Different Gray Zone Treatments in WRF-LES Real Case Simulations, Wind Energ. Sci. Discuss., https://doi.org/10.5194/wes-2017-5161, 2018, 10.1146/annurev.fluid.35.101101.161147, 2018.

Ghannam, K., Poggi, D., Porporato, A., and Katul, G. G.: The Spatio-temporal Statistical Structure and Ergodic Behaviour of Scalar Turbulence Within a Rod Canopy, Boundary-Layer Meteorology, 157, 447-460, 10.1007/s10546-015-0073-1, 2015.

Jarrin, N., Benhamadouche, S., Laurence, D., and Prosser, R.: A synthetic-eddy-method for generating inflow conditions for large-eddy simulations, International Journal of Heat and Fluid Flow, 27, 585-593, 10.1016/j.ijheatfluidflow.2006.02.006, 2006.

Keating, A., Piomelli, U., Balaras, E., and Kaltenbach, H. J.: A priori and a posteriori tests of inflow conditions for large-eddy simulation, Physics of Fluids, 16, 4696-4712, 10.1063/1.1811672, 2004.

Kempf, A., Klein, M., and Janicka, J.: Efficient generation of initial- and inflow-conditions for transient turbulent flows in arbitrary geometries, Flow Turbulence and Combustion, 74, 67-84, 10.1007/s10494-005-3140-8, 2005.

Kerschen, G., Golinval, J. C., Vakakis, A. F., and Bergman, L. A.: The method of proper orthogonal decomposition for dynamical characterization and order reduction of mechanical systems: An overview, Nonlinear Dynamics, 41, 147-169, 10.1007/s11071-005-2803-2, 2005.

Kim, Y., Castro, I. P., and Xie, Z. T.: Divergence-free turbulence inflow conditions for large-eddy simulations with incompressible flow solvers, Computers & Fluids, 84, 56-68, 10.1016/j.compfluid.2013.06.001, 2013.

Kim, Y., and Xie, Z. T.: Modelling the effect of freestream turbulence on dynamic stall of wind turbine blades, Computers & Fluids, 129, 53-66, 10.1016/j.compfluid.2016.02.004, 2016.

Klein, M., Sadiki, A., and Janicka, J.: A digital filter based generation of inflow data for spatially developing direct numerical or large eddy simulations, Journal of Computational Physics, 186, 652-665, 10.1016/s0021-9991(03)00090-1, 2003.

Kraichnan, R. H.: Diffusion by a Random Velocity Field, Physics of Fluids, 13, 22-31, 10.1063/1.1692799, 1970.

Laraufie, R., Deck, S., and Sagaut, P.: A dynamic forcing method for unsteady turbulent inflow conditions, Journal of Computational Physics, 230, 8647-8663, 10.1016/j.jcp.2011.08.012, 2011.

Lee, S., Lele, S. K., and Moin, P.: Simulation of spatially evolving turbulence and the applicability of Taylor's hypothesis in compressible flow, Physics of Fluids A-Fluid Dynamics, 4, 1521-1530, 10.1063/1.858425, 1992.

https://doi.org/10.5194/gmd-2019-165
Preprint. Discussion started: 22 July 2019

Lund, T. S., Wu, X. H., and Squires, K. D.: Generation of turbulent inflow data for spatially-developing boundary layer simulations, Journal of Computational Physics, 140, 233-258, 10.1006/jcph.1998.5882, 1998.

Ma, Y. L., and Liu, H. P.: Large-Eddy Simulations of Atmospheric Flows Over Complex Terrain Using the Immersed-Boundary Method in the Weather Research and Forecasting Model, Boundary-Layer Meteorology, 165, 421-445, 10.1007/s10546-017-0283-9, 2017.

Mirocha, J., Kosovic, B., and Kirkil, G.: Resolved Turbulence Characteristics in Large-Eddy Simulations Nested within Mesoscale Simulations Using the Weather Research and Forecasting Model, Monthly Weather Review, 142, 806-831, 10.1175/mwr-d-13-00064.1, 2014.

Moeng, C. H., Dudhia, J., Klemp, J., and Sullivan, P.: Examining two-way grid nesting for large eddy simulation of the PBL using the WRF model, Monthly Weather Review, 135, 2295-2311, 10.1175/mwr3406.1, 2007.

Morgan, B., Larsson, J., Kawai, S., and Lele, S. K.: Improving Low-Frequency Characteristics of Recycling/Rescaling Inflow Turbulence Generation, Aiaa Journal, 49, 582-597, 10.2514/1.j050705, 2011.

Munoz-Esparza, D., Kosovic, B., Mirocha, J., and van Beeck, J.: Bridging the Transition from Mesoscale to Microscale Turbulence in Numerical Weather Prediction Models, Boundary-Layer Meteorology, 153, 409-440, 10.1007/s10546-014-9956-9, 2014.

Munoz-Esparza, D., Kosovic, B., van Beeck, J., and Mirocha, J.: A stochastic perturbation method to generate inflow turbulence in large-eddy simulation models: Application to neutrally stratified atmospheric boundary layers, Physics of Fluids, 27, 10.1063/1.4913572, 2015.

Munters, W., Meneveau, C., and Meyers, J.: Turbulent Inflow Precursor Method with Time-Varying Direction for Large-Eddy Simulations and Applications to Wind Farms, Boundary-Layer Meteorology, 159, 305-328, 10.1007/s10546-016-0127-z, 2016.

Nottrott, A., Kleissl, J., and Keeling, R.: Modeling passive scalar dispersion in the atmospheric boundary layer with WRF large-eddy simulation, Atmospheric Environment, 82, 172-182, 10.1016/j.atmosenv.2013.10.026, 2014.

Nunalee, C. G., Kosovic, B., and Bieringer, P. E.: Eulerian dispersion modeling with WRF-LES of plume impingement in neutrally and stably stratified turbulent boundary layers, Atmospheric Environment, 99, 571-581, 10.1016/j.atmosenv.2014.09.070, 2014.

PALM, https://palm.muk.uni-hannover.de/trac/changeset/2259, 10.1016/j.compfluid.2014.11.005, 2017.

Schluter, J. U., Pitsch, H., and Moin, P.: Large eddy simulation inflow conditions for coupling with Reynolds-averaged flow solvers, Aiaa Journal, 42, 478-484, 10.2514/1.3488, 2004.

Skamarock, W. C., and Klemp, J. B.: A time-split nonhydrostatic atmospheric model for weather research and forecasting applications, Journal of Computational Physics, 227, 3465-3485, 10.1016/j.jcp.2007.01.037, 2008.

Tabor, G. R., and Baba-Ahmadi, M. H.: Inlet conditions for large eddy simulation: A review, Computers & Fluids, 39, 553-567, 10.1016/j.compfluid.2009.10.007, 2010.

Wu, X. H.: Inflow Turbulence Generation Methods, in: Annual Review of Fluid Mechanics, Vol 49, edited by: Davis, S. H., and Moin, P., Annual Review of Fluid Mechanics, 23-49, 2017.

Xie, Z. T., and Castro, I. P.: Efficient generation of inflow conditions for large eddy simulation of street-scale flows, Flow Turbulence and Combustion, 81, 449-470, 10.1007/s10494-008-9151-5, 2008.

Xie, Z. T., and Castro, I. P.: Large-eddy simulation for flow and dispersion in urban streets, Atmospheric Environment, 43, 2174-2185, 10.1016/j.atmosenv.2009.01.016, 2009.